



ELSEVIER

Surface Science 395 (1998) 148–167

surface science

# Surface corrugation effects: molecular ethane adsorption dynamics on rigid adsorbate-covered surfaces of Pt(111)

James A. Stinnett, Jason F. Weaver, Robert J. Madix \*

*Department of Chemical Engineering, Stanford University, Stanford, CA 94305, USA*

Received 18 March 1997; accepted for publication 23 April 1997

## Abstract

Angular distributions of ethane molecules scattered from sulfur- and ethylidyne-covered Pt(111), and clean Pt(111) were measured at surface temperatures of 135 and 210 K. Direct-inelastic scattering from the adsorbate-covered surfaces displays dramatic, broad back-scattering of ethane, while the clean surface produces maximum scattering intensity near the specular angle. Stochastic trajectory simulations for ethane on Pt(111)-S employing a potential developed from the trapping of ethane on Pt(111) gives a quantitative account of the broad angular distributions and the measured initial trapping probabilities at all energies and polar angles of incidence studied. The simulations clearly suggest facile interconversion of the incident parallel and perpendicular momenta of ethane upon the first collision with Pt(111)-S, which enhances trapping relative to clean Pt(111) at normal incidence, but increases scattering at more glancing angles. The simulations indicate the trapping probabilities for ethane on Pt(111)-S are determined to within 20% by the fate of the first bounce. Analysis of a large number of trajectories illustrates that at all angles of incidence, ethane is steered by the corrugation of the surface toward the bare platinum regions, producing both the broad angular distributions of the scattered species and the weak dependence of the trapping probability on the angle of incidence. © 1998 Elsevier Science B.V.

**Keywords:** Adsorption kinetics; Alkanes; Atom–solid interactions; Catalysis; Computer simulations; Low index single crystal surfaces; Molecular dynamics; Platinum

## 1. Introduction

Understanding the effects of adsorbates on metal surfaces on atomic/molecular adsorption is important since in most practical processes the surface is at least partially covered by adsorbed species. Well-controlled examinations of the nature of energy dissipation between a gas and an adsorbate-covered metal surface, however, date back only a little over a decade [1–18]. Early theoretical investigations by Adams et al. and Zhao et al. clearly

suggested profound enhancement of rare gas adsorption on partially covered surfaces [1–3]. The lack of significant experimental data on this subject at the time, however, left these calculations untested for several years. Experiments have since followed [4–18], yet currently a detailed understanding of the diverse mechanisms which govern adsorption on covered surfaces remains elusive. Consequently, in this study we present experimental results for ethane collisions with sulfur- and ethylidyne-covered Pt(111) and stochastic trajectory simulations for ethane adsorbing on Pt(111)-S which clearly illustrate the effects of a rigid overlayer on adsorption.

While in almost every case studied adsorbates

\* Corresponding address. Fax: (+1) 415 723 9780;  
e-mail: rjm@rio.stanford.edu.

are found to enhance adsorption on covered surfaces relative to the corresponding clean surfaces [1–16], the potential corrugation produced by the overlayer has been found to be substantially different, even for adsorbates which would appear to be similar (rare gases) [2,3,9–11]. The theoretical study by Zhao et al. suggested a monolayer of argon adatoms on W(110) presents a smooth effective surface corrugation to impinging argon atoms [2,3]. More recent simulations of argon trapping on argon-covered Ru(001) by Head-Gordon et al. indicated a high degree of corrugation which decreased with increasing incident energy,  $E_T$ , due to adsorbate recoil [11]. Experiments of xenon on xenon-covered Pt(111), also indicated a highly corrugated surface potential, since the xenon adsorption probability was found to be independent of angle of incidence,  $\theta_i$ ; yet the degree of surface corrugation was found to remain constant over the entire range of incident energies studied [9].

These somewhat conflicting findings signaled the need for both more experimental and theoretical information on adsorption. The molecular adsorption probability of ethane on clean [19] and ethane-saturated [8] Pt(111) was examined experimentally by Arumainayagam et al. as a function of  $E_T$  and  $\theta_i$  at a surface temperature of 95 K. Consistent with the notion that adsorbates produce more efficient energy transfer, adsorption of ethane on the ethane-covered Pt(111) surface was found to be enhanced relative to that on clean Pt(111). The initial adsorption probabilities,  $\alpha$ , for ethane on the clean surface scaled monotonically as  $E_T \cos^n \theta_i$ , with  $n=0.6$ , while on the ethane-covered surface adsorption scaled with  $n=0$ , consistent with a more corrugated gas–surface potential in the presence of adsorbate [20].

We have recently quantitatively reproduced the dependence of  $\alpha$  on  $E_T$  and  $\theta_i$  for ethane on clean Pt(111) [21] by employing an empirically determined pairwise Morse potential in stochastic trajectory simulations. Furthermore, with this potential we have predicted [22,23] the initial molecular trapping probabilities of methane [24] and propane [12] on Pt(111), and ethane [22] and propane [13] on Pt(110)-(1 × 2) without adjusting the Morse parameters. The success of these predic-

tions gives us confidence of the utility of this potential for trajectory simulations for ethane scattering from adsorbate-covered surfaces.

In early work the enhancement of the trapping probability of ethane on adsorbate-covered surfaces was attributed partially to increased mass matching between the colliding partners. Two recent studies, however, have revealed that adsorption on adsorbate-covered surfaces is not necessarily enhanced relative to the clean surface [17,18]. Soulen et al. demonstrated that a monolayer of hydrogen on Pt(111) reduces the initial adsorption probability of ethane by as much as 25% relative to the clean surface [17]. This effect was attributed to decreased energy transfer in the gas–surface collision due to stiffening of the platinum bonds from the adsorption of hydrogen. Quite unexpectedly, because the mass of sulfur is comparable to that of ethane, we have observed recently that the probability for the molecular adsorption of ethane on sulfur-covered Pt(111) is also decreased relative to clean Pt(111) at glancing angles of incidence [18]. This observation is certainly inconsistent with the idea of mass-matching as the origin of enhanced trapping. Adsorbed ethylidyne, however, does enhance trapping relative to clean Pt(111) for all incident conditions [18]. The disparity between ethane trapping on sulfur- and ethylidyne-covered Pt(111) was attributed to additional energy transfer to the internal degrees of freedom existent in adsorbed ethylidyne, such as low frequency frustrated translations and rotations [25].

In this paper we report measurements of the angular distributions of ethane scattered from Pt(111)–S and Pt(111)–CCH<sub>3</sub> [26], and stochastic trajectory simulations for ethane adsorbing on Pt(111)–S which illuminate some of the significant features of adsorption on adsorbate-covered metal surfaces. We show that the experimental results for ethane scattering and adsorption on Pt(111)–S can be accounted for by simply incorporating sulfur as an adsorbate and using the ethane–Pt potential [21] previously derived.

## 2. Experimental

Since the molecular beam apparatus employed in this study has been described in detail elsewhere

[26], only a brief description is provided here. It consists of an ultrahigh-vacuum (UHV) scattering chamber coupled to a triply differentially pumped supersonic molecular beam source. An ethane beam (Matheson, 99.99% purity) directed toward the Pt(111) crystal was passed through a modulation chamber which contains a 50% duty chopper for beam modulation and a solenoid-activated shutter to block or allow passage of the beam into the scattering chamber. The UHV chamber is pumped by turbo-molecular, ion and titanium sublimation pumps. These pumps are capable of producing a base pressure of  $5 \times 10^{-11}$  Torr and a pumping speed for ethane of  $800 \text{ l s}^{-1}$ .

The UHV chamber is equipped with low energy electron diffraction (LEED) and Auger electron spectroscopy (AES). The scattering chamber also contains two quadrupole mass spectrometers; one is rotatable about the crystal at a fixed distance of 12.1 cm and is used for direct trapping probability experiments (DTPE), in-plane angular distributions (AD), and time of flight measurements (TOF). The other mass spectrometer can be positioned near the crystal with a bellows and used for temperature-programmed desorption (TPD). In addition, a gold-plated flag positioned along the beam axis in the UHV chamber is used to block passage of the beam to the crystal.

The Pt(111) crystal was cleaned by argon ion sputtering with 10–15  $\mu\text{A}$  ion current and employing a 300–400 V bias on the crystal at a surface temperature of 300 K. The temperature was measured by a chromel–alumel thermocouple spot-welded to the back of the crystal. After it was sputtered, order was restored to the surface by annealing at 1400 K for 8 min. In addition, oxygen titration cycles, consisting of a 3 L ( $1 \text{ L} = 10^{-6} \text{ Torr} \cdot \text{sec}$ ) background dose of oxygen followed by heating to 1000 K, were performed until AES indicated that no contaminants were present above the noise level ( $< 0.02 \text{ ML}$ ). This procedure produced a hexagonal  $p(1 \times 1)$  LEED pattern.

The adsorbate-covered surfaces of sulfur [27–33] and ethylidyne [34–52] were prepared according to well-established procedures. A sulfur-covered surface was prepared by exposing clean Pt(111) to a 9 L background dose of  $\text{H}_2\text{S}$  at a surface temperature of 95 K, whereas ethylidyne-

covered Pt(111) was made by a 2 L background dose of  $\text{C}_2\text{H}_4$ . Subsequent heating of these surfaces to 350 and 550 K, produced hydrogen desorption near 270 and 230 K and well-ordered  $p(2 \times 2)$  and  $(\sqrt{3} \times \sqrt{3})\text{R}30^\circ$  LEED patterns for Pt(111)– $\text{CCH}_3$  and Pt(111)–S, respectively. A more complete description of the preparation methods of these adsorbate-covered surfaces is given elsewhere [18].

In-plane angular distributions of ethane scattering from clean Pt(111), Pt(111)–S and Pt(111)– $\text{CCH}_3$  were measured for surface temperatures of  $135 \pm 3$  and  $210 \pm 3$  K using phase sensitive detection (PSD) techniques with the rotary mass spectrometer [53,54]. The angular resolution was  $3^\circ$  as determined by the FWHM of a specularly scattered thermal He beam. The molecular beam was modulated at  $630 \pm 2$  Hz. Using the demodulation factor presented by D'Evelyn et al. [4] and the measured desorption energies for ethane on these surfaces [18,19], surface temperatures of 135 and 210 K correspond to demodulation factors of 0.03 and 0.99, respectively. Thus, at the higher surface temperature (210 K), both the direct-inelastic scattering and trapped-desorbed components of ethane were detected because the duration of trapped ethane molecules on these surfaces ( $0.9\text{--}9.0 \mu\text{s}$  for all three surfaces) was much less than the modulation period (1.6 ms). Conversely, at the lower surface temperature (135 K) only scattering in the direct-inelastic channel was measured because the trapped-desorbed component was demodulated. Angular distributions from the three surfaces were measured for ethane incident with  $30 \pm 3 \text{ kJ mol}^{-1}$  of initial translational energy at  $45^\circ$  with respect to the surface normal. The incident translational energies of ethane molecular beams were set by seeding ethane in helium and measured by PSD. To eliminate variation of vibrational energy distributions of incident ethane, the nozzle temperature was held constant at 300 K.

Following the measurement of the angular distributions of ethane from each of the three surfaces, DTPE, AES, and LEED experiments were performed. DTPEs performed with a modified King and Wells technique [19] at a surface temperature of 95 K after each measured angular distribution

showed excellent agreement ( $\pm 0.03$ ) with the values for  $\alpha$  cited in previous studies [18,19]. Auger spectra taken after each angular distribution showed no carbon accumulation, indicating that direct collisional activation of ethane did not occur. Finally, LEED performed after each covered-surface angular distribution showed that these surfaces retained the  $(\sqrt{3} \times \sqrt{3})R30^\circ$  and  $p(2 \times 2)$  patterns expected for sulfur- and ethylidyne-covered Pt(111), respectively.

### 3. Experimental results

The in-plane angular distributions of ethane molecules scattered from sulfur- and ethylidyne-covered Pt(111) surfaces at 210 K are significantly different from those observed for clean Pt(111) at the same surface temperature (Fig. 1). While the angular distributions of ethane from clean Pt(111) clearly shows both a direct-inelastic lobe peaked near the specular angle and a trapped-desorbed component centered at the surface normal, the angular distributions of ethane from both adsorbate-covered surfaces of Pt(111) exhibit a single broad peak near the surface normal. These very broad angular distributions, although somewhat surprising, are very reproducible. Furthermore, because the measured trapping probabilities of ethane on the adsorbate-covered surfaces are comparable to or greater than those for ethane on clean Pt(111), and since the angular distributions were performed such that both the direct-inelastic and trapped-desorbed components were detected, the angular distributions for ethane scattering/desorbing from sulfur- and ethylidyne-covered Pt(111) must contain both channels. The resolution of these components is discussed below.

In order to estimate only the direct-inelastic lobe, the angular distributions at 210 K were fit empirically to the sum of a cosine and a lobular channel (Fig. 1) and then compared to the measured angular distributions at 135 K (Fig. 2). A cosine channel centered at the surface normal was used to approximate the trapped-desorbed component of ethane at 210 K from each of the three surfaces. Since the initial trapping probabilities of

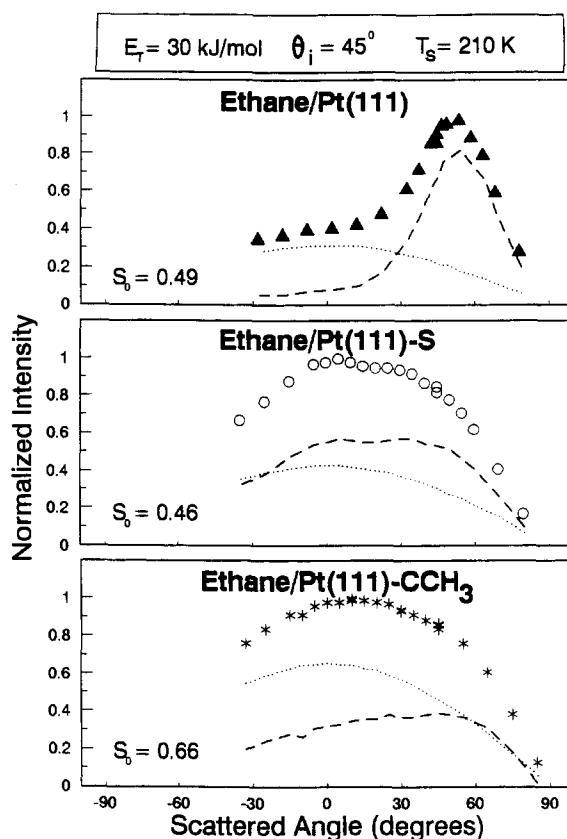


Fig. 1. Angular distributions of ethane scattering from Pt(111), Pt(111)-S and Pt(111)-CCH<sub>3</sub> at a surface temperature of 210 K from ethane incident with 30 kJ mol<sup>-1</sup> of initial translational energy at 45° from the surface normal. The symbols (solid triangles, open circles and asterisks) represent the experimental data, the dashed and dotted lines represent the estimated direct-inelastic and trapped-desorbed components of ethane, respectively. The initial trapping probabilities [18,19] of ethane on each surface are stated.

ethane on these surfaces have been measured previously at a surface temperature of 95 K [18,19], the relative fractions of these components are known. Consequently, the cosine channel was fit such that the relative areas under the direct-inelastic and trapped-desorbed components of each angular distribution gave a ratio consistent with the previously determined initial trapping probabilities. In doing so we realize the out-of-plane angular distribution of the lobular peak may actually be overestimated [55,56], especially for ethane scattering from clean Pt(111), which displays a

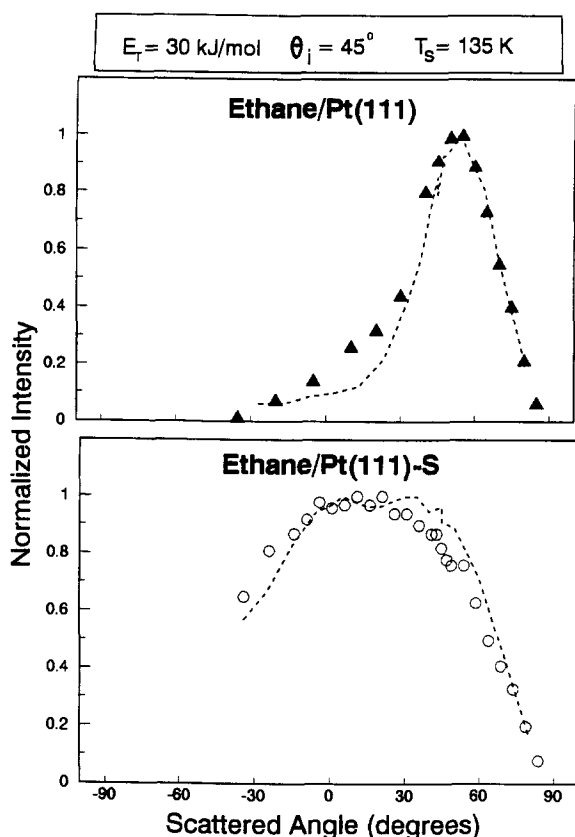


Fig. 2. Angular distributions of ethane scattering from Pt(111) and Pt(111)-S at a surface temperature of 135 K from ethane incident with  $30 \text{ kJ mol}^{-1}$  of initial translational energy at  $45^\circ$  from the surface normal. The symbols (solid triangles and open circles) represent the experimental data at 135 K, the dashed lines represent the estimated direct-inelastic components of ethane from each surface at 210 K.

narrower in-plane lobular channel. The resulting normalized, deconvoluted direct-inelastic lobes for ethane scattering from Pt(111) and Pt(111)-S, however, agree very well with measured angular distributions at 135 K in which the adsorption/desorption channel is demodulated (Fig. 2). Unfortunately, an angular distribution for ethane scattering from Pt(111)-CCH<sub>3</sub> at 135 K was not measured, so this cross check is not available.

The broad direct-inelastic scattering of ethane from these adsorbate-covered surfaces clearly indicates a higher gas-surface potential corrugation than for clean Pt(111). While the direct-inelastic channel of ethane on clean Pt(111) is centered

near the specular angle, the adsorbate-covered surfaces show direct-inelastic scattering over a much broader range of angles with a larger degree of back-scattering. Moreover, the broad direct-inelastic component of scattering from the adsorbate-covered surfaces are consistent with the total energy scaling of  $\alpha$  observed for ethane on these surfaces. For both the measured angular distributions and initial trapping probabilities the results suggest a high degree of perpendicular and parallel momentum interchange [18]. Clearly the presence of the adsorbate strongly influences the dynamics of scattering and adsorption. Consequently, stochastic trajectory simulations of ethane trapping on Pt(111)-S were pursued in order to investigate the origins of these effects.

#### 4. Simulation methods

Classical molecular dynamics was used to simulate ethane trapping on Pt(111)-S by employing a stochastic technique which has been described in detail previously [57,58]. With this method periodic boundary conditions are imposed in the plane of the surface to create an infinite slab in the  $x$ - and  $y$ -directions. Friction, random and constraint forces are applied to the bottom layer of the slab to mimic the effect of missing bulk platinum atoms. For this calculation we used a Pt(111)-S slab consisting of four layers, with the topmost layer composed of 12 sulfur atoms and the next three layers composed of 36 platinum atoms in each layer (Fig. 3). The sulfur atoms were arranged according to the well-documented  $1/3 \text{ ML}$  coverage ( $\sqrt{3} \times \sqrt{3} \text{ R}30^\circ$  structure of Pt(111)-S [27–33], with the equilibrium positions of the sulfur atoms  $1.65 \text{ \AA}$  above the FCC hollow sites of the Pt(111) substrate [29,32]. Consistent with the findings of Stinnett et al., the equilibrium positions of the platinum atoms were assumed to be the bulk-terminated sites (Pt–Pt bond length of  $2.769 \text{ \AA}$ ) [21]. We now describe the potentials employed.

##### 4.1. Pt–Pt and Pt–S potentials

The sulfur and platinum atoms were allowed to vibrate about their equilibrium positions. The

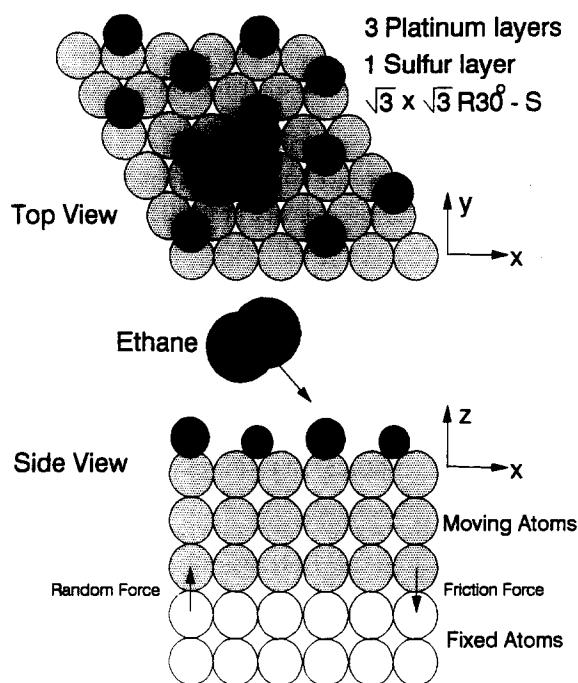


Fig. 3. Schematic illustrating the coordinate system used for the stochastic trajectory calculations. The Pt(111)–S slab consists of 120 atoms with 12 sulfur atoms in the first layer and 36 platinum atoms in each of the remaining three layers. Friction and random forces are added in the  $z$ -direction at the slab boundary to mimic the effect of the missing slab layers.

potential between platinum atoms was represented by nearest-neighbor (NN) and next nearest-neighbor (NNN) harmonic force constants. The parameters used were taken from previous work ( $k_{nn}=43.6 \text{ kg s}^{-2}$ ,  $k_{nnn}=10.2 \text{ kg s}^{-2}$ ) [59,60]. The friction constant applied to the fourth layer atoms in the  $z$ -direction was  $1.86 \times 10^{-13} \text{ s}^{-1}$ . The choice of these parameters follows the simple prescription proposed by Adelman and Doll for clean Pt(111) [61]. These slab parameters accurately reproduce the bulk Pt Debye temperature of 234 K [62,63]. The Pt–S potential was represented by in-plane and radial nearest-neighbor harmonic force constants. The radial force constant ( $153.3 \text{ kg s}^{-2}$ ) was set to reproduce the observed Pt–S vibrational frequency ( $375 \text{ cm}^{-1}$ ) from high-resolution electron energy loss spectroscopy (HREELS) [30], and the in-plane harmonic force constant ( $87.2 \text{ kg s}^{-2}$ ) was set to yield a Debye temperature near 500 K for adsorbed sulfur, as indicated by

the quantitative LEED analysis by Hayek et al. [29,32].

#### 4.2. Methyl–Pt and methyl–S potentials

Because of the excellent fit we were able to obtain between experiment and simulations for ethane adsorption on and scattering from Pt(111) [21] and the success of this potential for predicting the adsorption probabilities for ethane on Pt(110)–(1×2) [22], we used an analogous potential description for the ethane/Pt(111)–S interaction. Ethane was represented as a pseudo diatomic molecule composed of two methyl groups, and the gas–surface potential was taken to be the sum of the two methyl groups interacting with each of sulfur and platinum atoms. The potential for a single pairwise (methyl–platinum or methyl–sulfur) interaction is given by

$$V = \epsilon \{ \exp[-\sigma(r-r_0)] - 1 \}^2 - \epsilon \{ \exp[-\sigma(r_c-r_0)] - 1 \}^2, \quad r < r_c \quad (1)$$

$$V = 0, \quad r > r_c,$$

where the three parameters are:

- (i) the well depth  $\epsilon$ ;
- (ii) the position of potential minimum  $r_0$ ; and
- (iii) the range parameter  $\sigma$ .

The value of  $r_c$ , the cutoff distance outside of which the pair potential was taken to be zero, was set to  $9 \text{ \AA}$ , which is approximately half the slab width. Use of  $r_c$  is strictly for convenience to force the tail of the potential to zero beyond the cutoff distance. The distance  $r$  was taken to be the separation between a single methyl group and a surface atom or  $r_c$ , whichever was smaller. A sum for each methyl group over all surface atoms (sulfur and platinum) explicitly included in the slab was performed to obtain the total gas–surface potential.

The potential parameters determined to govern ethane trapping on and scattering from Pt(111) [21] were applied to the methyl–platinum and methyl–sulfur pairwise interactions of ethane with Pt(111)–S as follows. The methyl–platinum Morse potential parameters from the clean surface simulations were retained without change ( $r_0=3.1 \text{ \AA}$ ,  $\sigma=1.5 \text{ \AA}^{-1}$ ,  $\epsilon=2.53 \text{ kJ mol}^{-1}$ ) [21]. Likewise, rather

than optimizing the methyl–sulfur Morse parameters to match the experimental trapping probabilities of ethane on Pt(111)–S, these potential parameters were chosen by modifying the methyl–platinum parameters. Since the sulfur atomic radius is approximately 0.4 Å less than a platinum radius [28],  $r_0$  for the methyl–sulfur interaction was set to 2.7 Å. Because  $\sigma$  is related to the impulsiveness of the repulsion of the methyl group [21], the range parameter for the methyl–sulfur interaction was set to the same value as the methyl–platinum potential ( $\sigma = 1.5 \text{ Å}^{-1}$ ). The well depth  $\epsilon$  ( $1.22 \text{ kJ mol}^{-1}$ ) for the methyl–sulfur interaction was then adjusted to yield a total energy of adsorption of  $28 \text{ kJ mol}^{-1}$  on the Pt(111)–S surface, which is the experimental energy value [18].

#### 4.3. Methyl–methyl potential

Ethane was assumed to consist of two methyl groups bound by a Morse potential. The well depth was set at the C–C bond energy ( $\epsilon = 347 \text{ kJ mol}^{-1}$ ), and the distance at the potential minimum,  $r_0$ , was set at the center of mass methyl-to-methyl distance of ethane ( $r_0 = 1.7 \text{ Å}$ ). The range parameter for the methyl–methyl interaction was set to match the C–C vibrational frequency of  $1000 \text{ cm}^{-1}$  ( $\sigma = 2.0 \text{ Å}^{-1}$ ) [64]. Explicit inclusion of the hydrogens of ethane was assumed unnecessary since the much higher C–H vibrational frequency ( $3000 \text{ cm}^{-1}$ ) [64] would not be expected to be excited for the range of incident translational energies studied [19]. This assumption was supported by the fact that very little energy was found to be transferred to the C–C bond, which has a much lower frequency than the C–H bonds. Torsional excitation of the molecule was also neglected.

#### 4.4. Calculation method

Classical stochastic trajectories governed by the interactions described above were integrated by a modified Beeman algorithm with a time step of 2 fs [65]. The initial positions of the solid atoms were chosen to be the equilibrium positions. The initial momenta of the surface atoms were chosen at random for each trajectory from a Boltzmann

distribution at a prescribed surface temperature. Random forces at each integration step were selected from a Gaussian distribution which rigorously satisfies the fluctuation–dissipation theorem, as described previously [57].

Ethane molecules were initially located outside the range of the gas–surface interaction at 9.5 Å above the slab. The initial  $x$  and  $y$  center of mass positions of the molecule were chosen from a uniform random distribution covering the entire surface slab. The initial direction of the C–C bond axis was also chosen randomly. Initial rotational angular momenta were assigned at random from a Boltzmann distribution at an assumed initial rotational temperature. Since the experiments were conducted with a supersonic molecular beam which has substantial rotational cooling, a rotational temperature of 10 K was used. The initial center of mass translational energy of ethane was chosen to be monoenergetic, with the energy and angle chosen to match specific experimental conditions.

Trajectories were integrated until one of the three following conditions occurred. (1) The ethane molecule scattered from the surface and escaped to a height greater than the potential cutoff (10 Å). These trajectories were classified as scattered. (2) The total energy (kinetic plus potential) of ethane fell below  $-10k_bT_s$  per methyl group. These trajectories were designated as trapped. (3) If neither (1) nor (2) resulted after the 15000 integration steps (30 ps), the trajectory was terminated and classified as uncertain. The number of uncertain trajectories for each specific incident energy and angle was no greater than 0.1% (two trajectories); as a result, uncertain trajectories were discarded from analysis. Unless otherwise stated, all computed trapping probabilities were obtained from a sample of 2000 trajectories. This yields a statistical uncertainty in the calculated trapping probabilities of  $\pm 0.02$ .

### 5. Simulation results

#### 5.1. Initial trapping probability

The predicted initial trapping probabilities for ethane on Pt(111)–S at a surface temperature of

95 K agree very well with the experimental results determined previously [18] (Table 1). For the range of incident angles and translational energies studied, the theoretical values for  $\alpha$  differ by no more than 10% to the experimental initial trapping probabilities. Furthermore, the calculations indicate that the adsorption probability is very insensitive to the angle of incidence, scaling according to  $E_T \cos^{0.2}\theta_i$ , which is very near the experimentally determined energy scaling exponent for ethane trapping on Pt(111)-S,  $n=0$  (Fig. 4). The excellent quantitative agreement between theory and experiment in both the magnitude of  $\alpha$  and the energy scaling indicates the gas-surface potential corrugation for the simulations of ethane on Pt(111)-S is reasonably well represented by the model chosen.

The simulations also predict the correct differences between  $\alpha$  for ethane on Pt(111)-S and Pt(111) (Fig. 5). For ethane incident with an initial translational energy of 40 kJ mol<sup>-1</sup>, the values of  $\alpha$  predicted for ethane on Pt(111)-S are larger at normal incidence and smaller at 60° relative to the initial trapping probabilities simulated for ethane on Pt(111). These findings are consistent with the

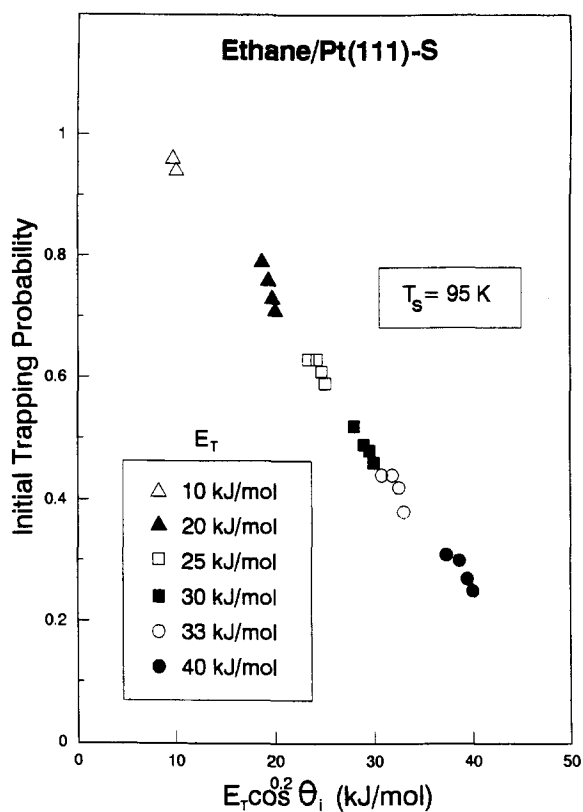


Fig. 4. The simulated initial trapping probabilities of ethane on Pt(111)-S at a surface temperature of 95 K plotted as a function of  $E_T \cos^{0.2}\theta_i$ .

Table 1

Table of initial trapping probabilities from experiment and stochastic trajectory simulation for ethane on Pt(111)-S at a surface temperature of 95 K

$E_T$ (kJ mol <sup>-1</sup> )	$\theta_i$ (degrees)	$\alpha$ (experiment)	$\alpha$ (theory)
10	0	0.85	0.94
10	45	0.85	0.96
20	0	0.72	0.71
20	30	0.73	0.73
20	45	0.72	0.76
20	60	0.72	0.79
26	0	0.61	0.59
26	30	0.62	0.61
26	45	0.61	0.63
26	60	0.60	0.63
30	0	0.45	0.46
30	30	0.46	0.48
30	45	0.46	0.49
30	60	0.48	0.52
40	0	0.31	0.25
40	30	0.30	0.27
40	45	0.30	0.30
40	60	0.30	0.31

experimental results for ethane on clean and sulfur-covered Pt(111), suggesting that the important mechanisms for the adsorption of ethane on Pt(111) and Pt(111)-S have been adequately incorporated into the model. Previous simulations did not indicate reduction of the trapping probability on covered surfaces [1–3,11,12,16].

Interestingly, the simulations indicate the relative difference between the trapping probabilities for ethane on Pt(111) and Pt(111)-S will continue to increase for angles greater than 60° (Fig. 5).<sup>1</sup> Consistent with the observed energy scaling of  $\alpha(n=0.6)$  for angles from 0 to 60°, predictions for

<sup>1</sup> Unlike actual experiments which are limited by the size of the crystal relative to the incident molecular beam, simulations, which employ an essentially infinitely large crystal, allow for the prediction of the trapping probabilities over a wider range of incident angles.



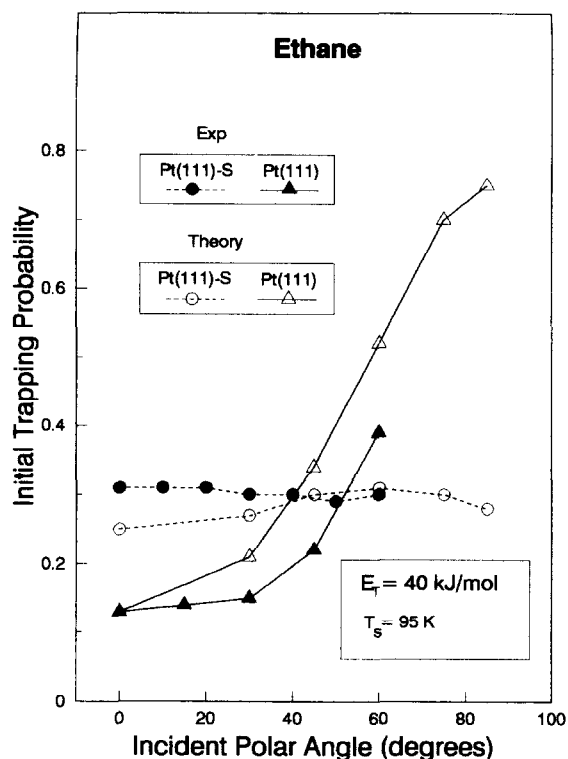


Fig. 5. The initial trapping probabilities of ethane on Pt(111) and Pt(111)-S at a surface temperature of 95 K as a function of polar angle ( $\theta_i$ ) ethane incident with  $E_T = 40 \text{ kJ mol}^{-1}$ . The solid symbols represent the experimental data [18] and the open symbols are from the simulations.

ethane trapping on clean Pt(111) suggest  $\alpha$  continues to increase with increasing angle. The observed total energy scaling of  $\alpha$  for ethane on Pt(111)-S is predicted to extend to at least  $85^\circ$ . This result clearly suggests that parallel momentum exchange is participating in the trapping mechanism of ethane on Pt(111)-S, since an ethane beam incident at  $85^\circ$  has less than 1% of its initial translational energy in momentum directed perpendicular to the surface.

## 5.2. Angular distributions

The good agreement with the measured dependence of the initial trapping probability for ethane on  $E_T$  and  $\theta_i$  on sulfur-covered Pt(111) indicates that the gas-surface potential utilized provides a

reasonable basis for understanding the gross features of the gas-surface collision; the success of the predictions of angular distributions for ethane from Pt(111)-S lends further support to this suggestion (Fig. 6). The in-plane angular distribution of scattered ethane molecules from sulfur-covered Pt(111) is predicted to be quite broad, peaked near the surface normal with a high degree of back-scattering, in agreement with experiment (Figs. 1 and 2).

Simulations of the in-plane angular distributions

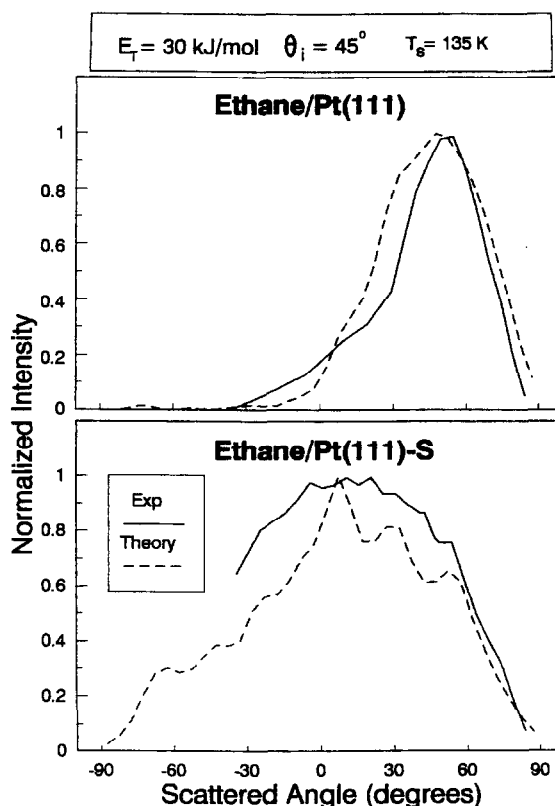


Fig. 6. Angular distributions of ethane scattering from Pt(111) and Pt(111)-S at a surface temperature of 135 K from ethane incident with  $30 \text{ kJ mol}^{-1}$  of initial translational energy at  $45^\circ$  from the surface normal. The solid lines represent the demodulated angular distributions of ethane from each surface at 135 K. The dashed lines are the predicted angular distributions from simulations using 15 000 initial trajectories by considering only those trajectories which scatter in-plane to within  $\pm 5^\circ$ . More initial trajectories were used to ensure better statistics since only a fraction of the molecules scatter in-plane. For comparison the distributions have been normalized to the greatest intensity.

of scattered ethane molecules from clean Pt(111) and Pt(111)–S as a function of angle of incidence also indicate that the sulfur-covered surface scrambles the momenta of the incident ethane (Fig. 7). Indicative of retention of memory of its incident parallel momentum, the peak intensity in ethane scattering from clean Pt(111) shifts to the specular angle with changing angle of incidence, whereas the angular distributions for ethane scattered from sulfur-covered Pt(111) at 0 and 45° differ very little. Thus, while values of  $\alpha$  computed at 45° for each of these cases are nearly equal ( $0.51 \pm 0.02$ ), the angular distributions show clear differences in the retention of parallel and normal momentum on the two surfaces.

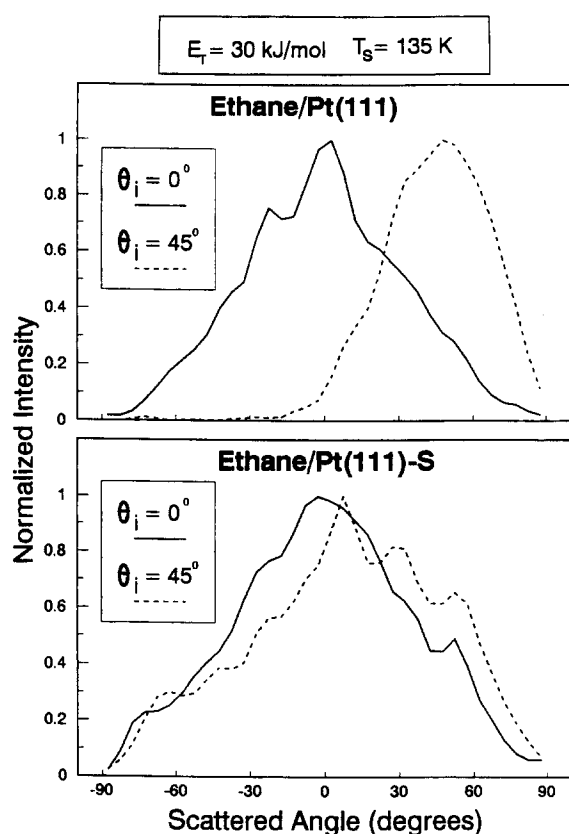


Fig. 7. Angular distributions of ethane scattering from Pt(111) and Pt(111)–S at a surface temperature of 135 K from ethane incident with  $30 \text{ kJ mol}^{-1}$  of initial translational energy at 0° (solid lines) and 45° (dashed lines) from the surface normal. 15 000 initial trajectories were used.

## 6. Discussion and analysis

In order to assess the energy transfer processes involved in the adsorption and scattering of ethane on sulfur-covered Pt(111), the partitioning of energy of each single trajectory was analyzed for the first two bounces after impact with the surface. At the point where ethane rebounded to either the scatter height or the classical turning point away from the surface<sup>2</sup> after its initial collision with the surface, the kinetic energies in helicopter and cartwheel motion,<sup>3</sup> in-plane and perpendicular translational motion, and the potential energy were evaluated and stored. The total amount of energy lost to surface phonons was evaluated by subtracting the sum of the five aforementioned energies from the initial kinetic (translational and rotational) energy.

If a given trajectory continued for a second surface collision, the same energy calculations were repeated at either the scatter height or outward turning point. In addition, if a trajectory proceeded beyond more than two surface collisions, the energy profile upon scattering or trapping was calculated when the trajectory was terminated. The number of surface collisions a trajectory experienced was also stored as information. Once all 2000 trajectories were finished, the average values of these energies after the first two bounces and the last surface collision were calculated.<sup>4</sup>

### 6.1. Comparison of surfaces

The partitioning of the initial translational energy after the first bounce suggests the origins of the differences in the initial trapping probabilities of ethane on Pt(111)–S and clean Pt(111)

<sup>2</sup> The classical turning point away from the surface is strictly defined as the point where the  $z$ -direction center of mass velocity of the molecule changes sign from positive to negative. The negative direction is into the surface.

<sup>3</sup> Helicopter motion is defined as rotation with the angular momentum vector ( $J$ ) directed along the surface normal ( $z$ -direction) while cartwheel motion is defined as rotation parallel to the surface ( $x$ – $y$  plane).

<sup>4</sup> This method of analysis was used previously to determine the relative roles of the energy storage mechanisms available to assist ethane trapping on Pt(111) [21] and Pt(110)–( $1 \times 2$ ) [22].

(Fig. 8a and b). For this discussion it is useful to think of perpendicular energy as the energy accessible to ethane for escape from the surface, and thus it is intimately tied to  $\alpha$ .

Contrasting amounts of interconversion of perpendicular and parallel translational energy after the first bounce account primarily for the differences in the trapping of ethane on Pt(111) and Pt(111)-S over the range of angles of incidence. At normal incidence, while the amounts of cartwheel and helicopter rotational excitations are nearly the same for each surface, the simulations reveal that even though less energy is lost to

phonons on the sulfur-covered surface, far more parallel energy is gained relative to the clean surface (Fig. 8a). The decrease in energy lost to phonons for ethane on Pt(111)-S is consistent with the suggestion from our previous study that excitation of the Pt-S vibration is unlikely [18]. Despite the reduction in phonon excitation, the corrugated sulfur-covered surface enhances trapping of ethane at  $0^\circ$  relative to Pt(111) by converting a larger amount of normal translational energy into parallel energy. The corrugation has the opposite effect for ethane incident on Pt(111)-S at  $60^\circ$ , at which the adsorption probability is less than on the clean surface. While the slight difference in energy transferred to helicoptering on the sulfur-covered surface assists trapping, the loss of parallel translational energy results in less trapping at this angle on sulfur-covered Pt(111) than on clean Pt(111) (Fig. 8b). The slightly larger helicopter excitation on Pt(111)-S is also consistent with a more corrugated surface [21].

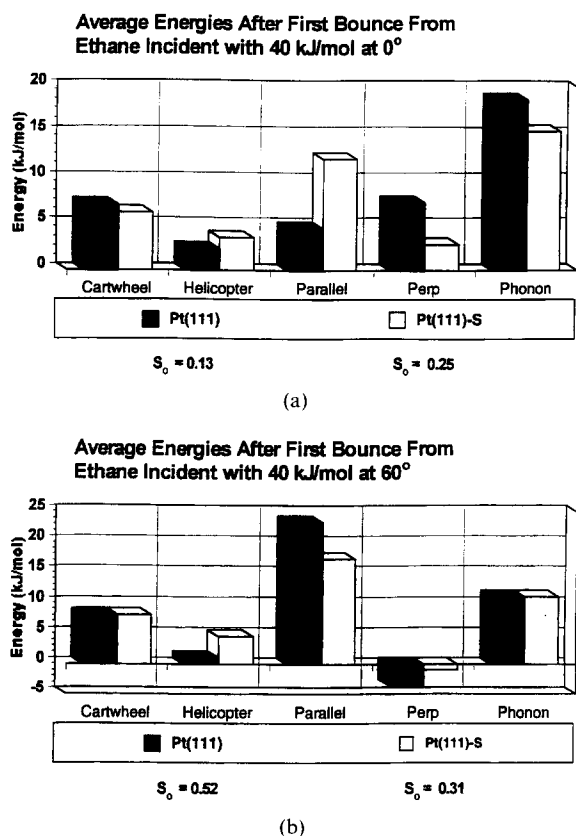


Fig. 8. The average energy profiles after the first bounce from ethane incident at Pt(111) and Pt(111)-S with  $40 \text{ kJ mol}^{-1}$  of initial translational energy (a) at normal incidence and (b) at  $60^\circ$ . Histograms for cartwheel rotational, helicopter rotational, parallel translational, perpendicular translational and surface phonon energies are shown. The calculated initial trapping probabilities from simulation at 95 K for each surface and incident condition are stated.

## 6.2. Energy channeling in trapping of ethane on Pt(111)-S

The conversion of perpendicular translational energy to parallel energy at normal incidence and the retention of parallel translational energy at glancing incidence are also the processes which discriminate trapping from scattering (Table 2). While at normal incidence the excitation of cartwheel and helicopter motions as well as surface phonons positively contribute to the trapping of ethane after the initial collision, the large difference in parallel energy between trapped and scattered trajectories accounts for over 50% of the difference in perpendicular energy between the two classes of collisions at incident energies of both 20 and  $40 \text{ kJ mol}^{-1}$ . Clearly, energy transfer from normal to parallel motion is the most significant single factor in trapping at this angle. For ethane incident at  $60^\circ$ , single bounce scattering is accompanied by a large loss of initial parallel momentum while temporarily trapped species retain over 75% of the initial value. Thus, at glancing incidence the energy retained in parallel momentum after the first bounce distinguishes trapping from scattering. The

Table 2

The averages of energies resulting from the first bounce for ethane incident at Pt(111)-S with 20 and 40 kJ mol<sup>-1</sup> at 0 and 60°. All energies are in kJ mol<sup>-1</sup>. Columns labeled “one bounce scattered” and “temporarily trapped” represent the average energies of trajectories that scatter after a single bounce and those that experience at least a second bounce, respectively. The column titled “difference” represents the difference between these averages. The negative sign for perpendicular energy indicates the molecule resides in the potential well of the surface

	Temporarily trapped	One bounce scattered	Difference
Normal incidence, 20 kJ mol <sup>-1</sup> ( $\alpha=0.71$ )			
Cartwheel	6.3	2.2	4.1
Helicopter	2.9	1.1	1.8
Parallel	10.3	3.2	7.1
Perpendicular	-9.7	3.9	-13.6
Phonon	10.2	9.6	0.6
Glancing incidence (60°), 20 kJ mol <sup>-1</sup> ( $\alpha=0.79$ )			
Cartwheel	6.9	2.5	4.4
Helicopter	3.1	1.7	1.4
Parallel	12.1	4.8	7.3
Perpendicular	-10.2	3.7	-13.9
Phonon	8.1	7.3	0.8
Normal incidence, 40 kJ mol <sup>-1</sup> ( $\alpha=0.25$ )			
Cartwheel	10.0	3.7	6.3
Helicopter	4.6	2.9	1.7
Parallel	19.1	7.3	11.8
Perpendicular	-7.9	10.3	-18.2
Phonon	14.2	15.8	-1.6
Glancing incidence (60°), 40 kJ mol <sup>-1</sup> ( $\alpha=0.31$ )			
Cartwheel	9.9	5.7	4.2
Helicopter	5.2	3.6	1.6
Parallel	22.8	10.3	12.5
Perpendicular	-8.5	9.0	-17.5
Phonon	106	114	-0.8

energy exchange processes which dictate trapping on the sulfur-covered surface are dissimilar from those important on clean Pt(111), on which cartwheel rotational excitation acts as the primary energy storage mechanism responsible for trapping [21]. However, they are very similar to those operative on Pt(110)-(1×2), which is also very corrugated [22]. The simplest explanation of the loss of parallel momentum at high angles is that the incident molecule scatters off the corrugation back into the gas phase with accompanying interconversion of parallel to normal momentum. This conclusion is supported by individual trajectories. The excitation of cartwheel motion also appears to be significant in trapping (Table 2). Helicopter and phonon excitation, however, while useful energy dissipation processes for promoting trapping, do not appear to differ much for trapped or scattered species. These energy channels either

involve small amounts of energy (helicopter) or receive about the same amount of energy (phonons). The importance of cartwheel rotational excitation in facilitating trapping is consistent with the well-documented rotationally mediated selective adsorption (RMSA) of hydrogen on various metal surfaces [66–76], and the concept of rotational trapping described in a theoretical investigation by Polanyi et al. and in several subsequent studies [77–84]. As the incident translational energy is increased to 40 kJ mol<sup>-1</sup>, the relative importance for each of the energy storage mechanisms at both angles of incidence remains essentially the same, but phonon excitation appears to contribute slightly less to trapping. The decrease in importance of phonons in producing trapping probably comes about from an anti-correlation between excitation of parallel translational energy and phonons, similar to the anti-correlation of

phonons with rotational energy observed by Rettner and co-workers [85,86].

To this point the discussion of channeling of incident energy into the various available energy storage mechanisms has focused on the first bounce. In our previous studies of alkanes on clean platinum surfaces we have suggested that the importance of multiple bounce scattering is limited, since computations indicate the initial trapping probability is determined to within 12% by the fate of the first gas-surface collision [21–23]. For ethane trapping on Pt(111)-S, however, the effect of subsequent bounces appears to be greater (Fig. 9).

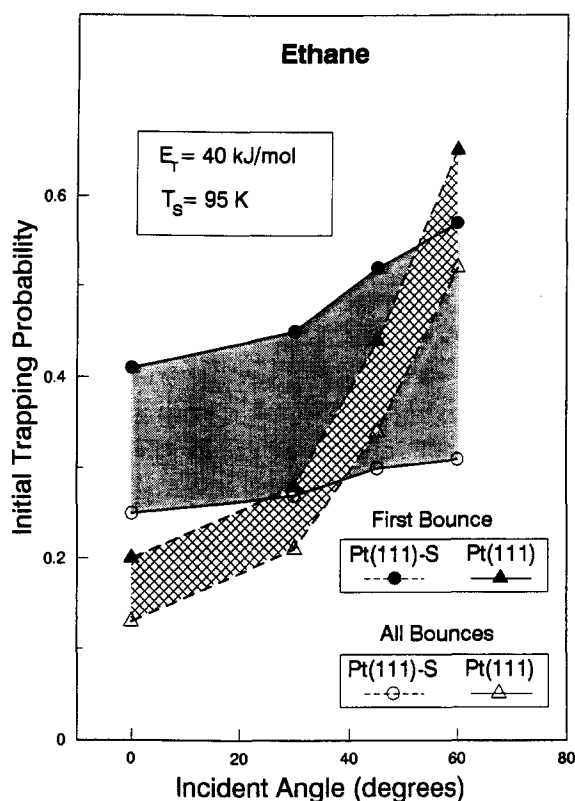


Fig. 9. The apparent trapping probabilities after the first surface bounce and the calculated initial trapping probabilities of ethane on Pt(111) (triangles) and Pt(111)-S (circles) plotted as a function of polar angle ( $\theta_i$ ) resulting from ethane incident with  $40 \text{ kJ mol}^{-1}$  of initial translational energy. The solid and open symbols represent the apparent values after the first bounce and the calculated values considering all bounces, respectively. The surface temperature is 95 K.

Reduction of the trapping probability due to scattering after more than one bounce on the surface is most significant at high incident translational energies where a greater fraction of energy must be dissipated to remain trapped. Multiple bounce scattering is also slightly more likely at glancing angles where the fraction of trajectories which scatter after successive impacts with the surface account for almost 20% of the total number of trajectories. Interestingly, for ethane incident at  $45^\circ$  with  $40 \text{ kJ mol}^{-1}$  of initial translational energy, the probability that it remains bound to the surface after the first bounce is greater on the sulfur-covered Pt(111) surface than on clean Pt(111), but it is less after all bounces. This result suggests that velocity distributions of ethane scattered from Pt(111)-S under these conditions should appear broader than analogous distributions from clean Pt(111).

Conversion of parallel translational momentum into perpendicular momentum is the primary mechanism which leads to multiple bounce scattering of ethane from Pt(111)-S (Fig. 10). Molecules at normal incidence with  $40 \text{ kJ mol}^{-1}$  of kinetic energy which scatter after two bounces lose almost  $15 \text{ kJ mol}^{-1}$  of parallel translational energy upon the second collision with surface, some of which is converted to perpendicular energy sufficient to allow scattering. Ethane which remains in the attractive part of the potential after the second bounce, however, dissipates parallel energy at a much slower rate, about  $2 \text{ kJ mol}^{-1}$  upon the second bounce. Molecules which scatter after more than two bounces suffer a similar collision to those which scatter upon two bounces, i.e. a large reduction in parallel translational momentum upon the final collision with the surface, while trapped ethane dissipates this energy through a cascade of surface collisions.

Furthermore, those which scatter by two or more bounces have on the average a larger amount of parallel translational energy after the first bounce than species which ultimately trap. This result suggest that although greater parallel energy clearly assists ethane to experience a second bounce, excessive parallel energy is likely to produce scattering on subsequent bounces. Ethane scattering via two or more bounces from the open

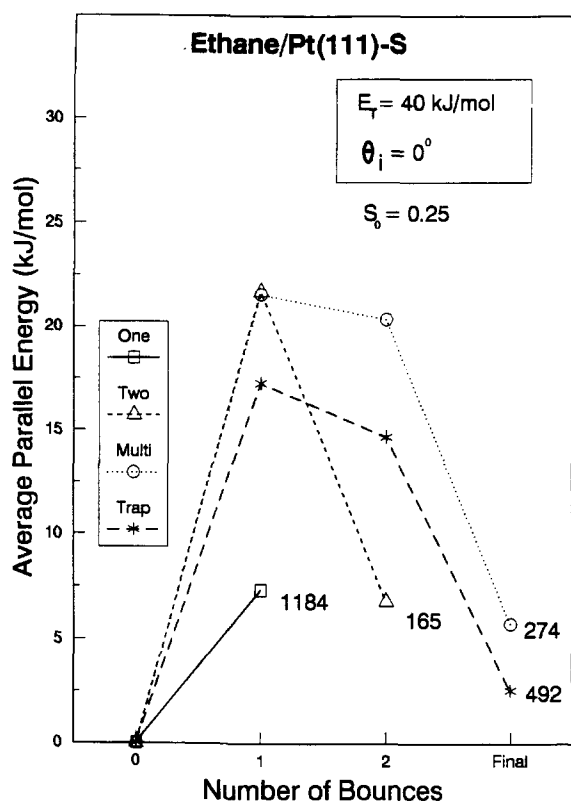


Fig. 10. The progress of average parallel translational energy as a function of number of bounces resulting from ethane incident at Pt(111)-S with  $40 \text{ kJ mol}^{-1}$  of translational energy at normal incidence. The open squares, open triangles, open circles and asterisks represent the average parallel translational energy for one bounce, two bounce, multiple (more than two bounces) bounce and trapped trajectories, respectively. The number besides each line represents the number of trajectories for that type of trajectory. The calculated value of the initial trapping probability at 95 K is stated. Two thousand initial trajectories were used.

surface of Pt(110)-(1 × 2) demonstrates analogous gas-surface dynamics [22], while on clean Pt(111) multiple bounce scattering appears to originate primarily from the deexcitation of excess rotational energy [21].

### 6.3. Site dependence

The trapping/scattering behavior can be strongly influenced by the site on which impact occurs [22,23,87,88]. Kummel and co-workers have shown that  $\text{N}_2$  beams incident at high angles on

Ag(111) scatter with fast forward cartwheel tumbling of the molecule for impacts on the shady side of a surface atom, while a slow backward cartwheel motion is more likely for impacts on the leading face [88]. Stinnett et al. demonstrated that the ridges of Pt(110)-(1 × 2) more effectively scatter ethane, while the troughs tend to promote adsorption [22]. Here we investigated the importance of impact sites for ethane trapping on Pt(111)-S both by computing site specific trapping probabilities and by creating impact site maps from a large number of randomly generated trajectories.<sup>5</sup>

While the trapping probability of ethane on clean Pt(111) shows essentially no dependence on the point of impact, the sulfur-covered Pt(111) surface exhibits a notable variance in  $\alpha$  with impact site, particularly with respect to the overlayer sulfur structure (Fig. 11). The trapping probability is least for trajectories which are directed toward and impact the atop sulfur site of Pt(111)-S. This finding is contrary to simple cube models [89–93] which would predict trapping to be greatest on the atop sulfur site due to a match in mass of gas-surface species. The fact that the trapping probability computed for the atop sulfur site is much lower than the value calculated for all trajectories also indicates the likelihood of actually striking the sulfur atom head-on may be quite low, and thus steering of incident ethane molecules may occur.<sup>6</sup>

Inspection of the center of mass positions at the inner turning points for ethane at 0 and  $60^\circ$  clearly reveals this dynamical effect (Fig. 12). Both incident conditions show preference for impact in the bare platinum regions of Pt(111)-S. The static surface potential energy plots for ethane inter-

<sup>5</sup> These methods are well described in the site dependence analysis of ethane trapping on Pt(110)-(1 × 2) [22]. The first method calculates site specific initial trapping probabilities by selectively directing the center of mass of ethane at normal incidence to specific well-defined surface sites of Pt(111)-S. The second method employs ethane directed at random sites, as usual, and maps out the continuous site dependence for ethane trapping on Pt(111)-S by storing the initial starting positions and the first inner turning points of each single trajectory.

<sup>6</sup> Impact site maps from our previous study found the open microstructure of Pt(110)-(1 × 2) steered incident ethane away from the ridges and toward the trough centers [22].

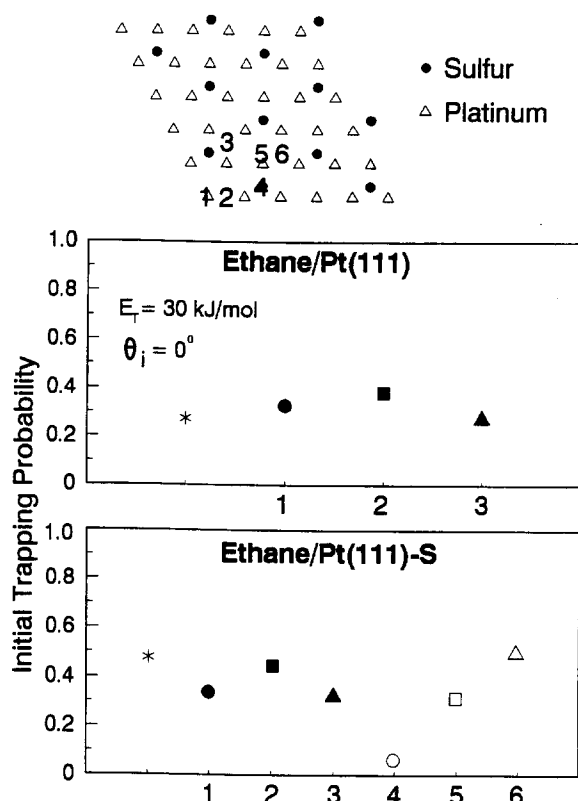


Fig. 11. The initial trapping probability from simulations of ethane incident with  $30 \text{ kJ mol}^{-1}$  of normal translational energy at Pt(111) and Pt(111)-S toward specific surface sites. The asterisks, solid circles, solid squares and solid triangles represent the initial trapping probabilities calculated for randomized sites, platinum atop, platinum bridge and platinum hollow, respectively. For the Pt(111)-S surface the open circle, open square and open triangle are for the sulfur atop, sulfur bridge and sulfur hollow sites, respectively. Each initial trapping probability calculation was performed for a surface temperature of 95 K by using 2000 trajectories.

acting with clean and sulfur-covered Pt(111) (Figs. 13a and b) clearly indicate the origin of this steering effect. While the sharp peaks in the potential energy surface of Pt(111) induce slight steering of incident ethane away from atop sites, the distance between platinum surface atoms ( $2.769 \text{ \AA}$ ) is too close to allow a methyl group ( $r_0 = 3.1 \text{ \AA}$ ) to significantly penetrate the regions of less repulsion (Fig. 13a). The larger spacing between sulfur atoms ( $4.796 \text{ \AA}$ ) on Pt(111)-S, however, enables a methyl group to be steered between the sulfur atoms where it experiences a reduced repulsion or,

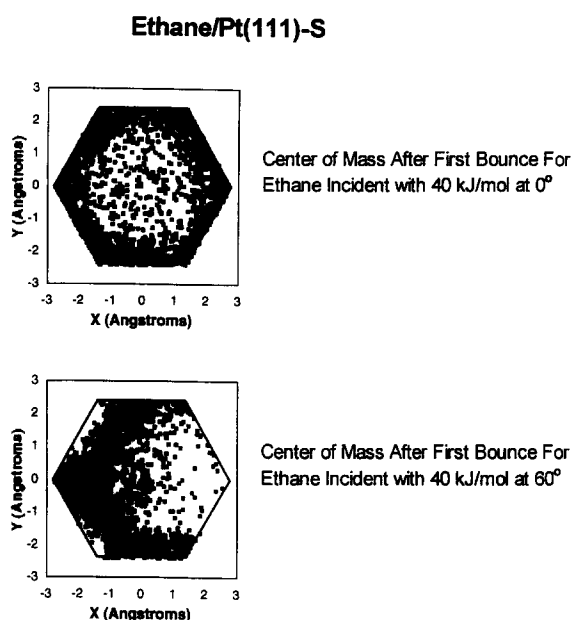


Fig. 12. The center of mass positions of all 2000 trajectories with respect to the closest sulfur atoms after the first bounce from ethane incident at Pt(111)-S with  $40 \text{ kJ mol}^{-1}$  of initial translational energy at  $0^\circ$  (upper panel) and  $60^\circ$  (lower panel). The direction of the beam for  $\theta_i = 60^\circ$  is from the left. The solid line around the data represent the Wigner-Seitz cell. Each dot represents a single trajectory. The sulfur atom is located at  $x = 0, y = 0$ .

quite possibly, attraction to the platinum atoms (Fig. 13b). Substantial steering for ethane at both  $0$  and  $60^\circ$  occurs because the energy of adsorption for ethane on Pt(111)-S ( $28 \text{ kJ mol}^{-1}$ ) is on the order of the maximum incident translational energy studied ( $40 \text{ kJ mol}^{-1}$ ). As a result, incident ethane has sufficient time to be repelled from the adsorbed sulfur atoms into “bare” regions at sufficient distances from the platinum atoms such that the forces have not yet become repulsive.

The steering of the incident ethane is an important factor in determining the total energy scaling of the initial trapping probabilities of ethane on Pt(111)-S. Unlike trajectories of ethane on clean Pt(111) which are steered negligibly and retain partial memory of the initial incident momentum after the first surface collision, the steering of ethane into the bare platinum regions of Pt(111)-S produces rapid scrambling of the incident momentum. As a result of this steering, collisions with

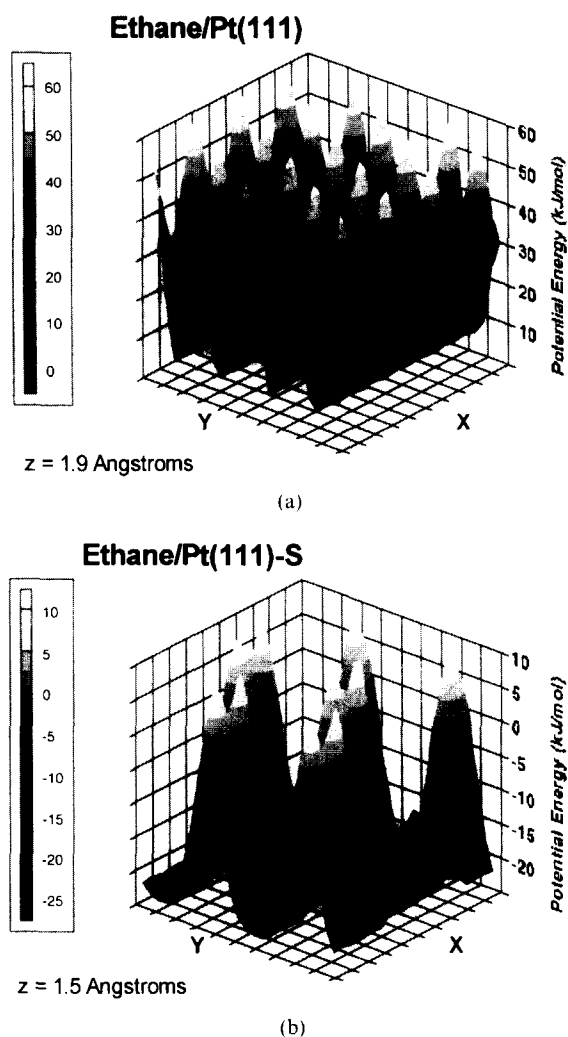


Fig. 13. The static surface potentials for ethane interacting with (a) clean Pt(111), and (b) Pt(111)-S. Ethane is oriented parallel to both surfaces at a heights of 1.9 Å for Pt(111) and 1.5 Å for Pt(111)-S, with the C-C bond directed along the  $x$ -axis. The potential energy was calculated for a  $10 \times 10$  Å grid. The different heights above the surface (1.5 and 1.9 Å) for the two potential energy surfaces were chosen due to different methyl-sulfur and methyl-platinum distance parameters (2.7 and 3.1 Å), thus allowing comparison of the surfaces.

the surface become singular for all angles of incidence. Consequently, ethane scattering from Pt(111)-S exhibits angular distributions nearly independent of incident angle, and the initial trapping probabilities of ethane on this surface should remain constant with angle; both these effects have

been confirmed experimentally. Indeed, the basic fact of total energy scaling suggests that for the diverse incident trajectories an event(s) occurs which causes an equivalence of the different paths. The steering of ethane from the corrugation of the sulfur atoms is such a phenomena. Interestingly, calculations of propane trapping on Pt(111)-S indicate the larger propane molecule is also steered by the sulfur corrugation and that total energy scaling of  $\alpha$  is predicted (J.A. Stinnett and R.J. Madix, preliminary results).

#### 6.4. Representative single trajectories

To further illustrate the role of corrugation on the trapping dynamics of ethane on Pt(111)-S, three single trajectories are presented and discussed (Figs. 14a–c and 15). All of the single trajectories were computed for a surface temperature of 95 K for ethane incident with  $33 \text{ kJ mol}^{-1}$  of translational energy; one trajectory is illustrated for an incident angle of  $45^\circ$  and two are given for  $0^\circ$ . While it should be noted that there is really no trajectory which can be considered as typical, these three illustrate the main features of ethane scattering on Pt(111)-S: namely, broad back-scattering, multiple bounce scattering and steering of ethane from the corrugation presented by sulfur.

Fig. 14a shows the energy profile of a single bounce, highly back-scattered trajectory. Examining the path of this trajectory in the  $x$ - $y$  plane (Fig. 15) reveals the scattered molecule is turned completely around by the corrugated Pt(111)-S surface. Further inspection of the path of this trajectory indicates ethane strikes a sulfur atom nearly head-on (Fig. 15). Impact of this nature produces large rapidly changing torques on the molecule causing its direction to be reversed (Fig. 14a). This type of trajectory is consistent with the broad angular distributions observed experimentally.

Fig. 14b illustrates a multiple bounce scattered trajectory of ethane from Pt(111)-S. Initially directed somewhat near the atop sulfur site (Fig. 15), the molecule is steered away from this site, which produces a rather large amount of conversion to parallel translational and rotational energies (Fig. 14b) and enables the molecule to



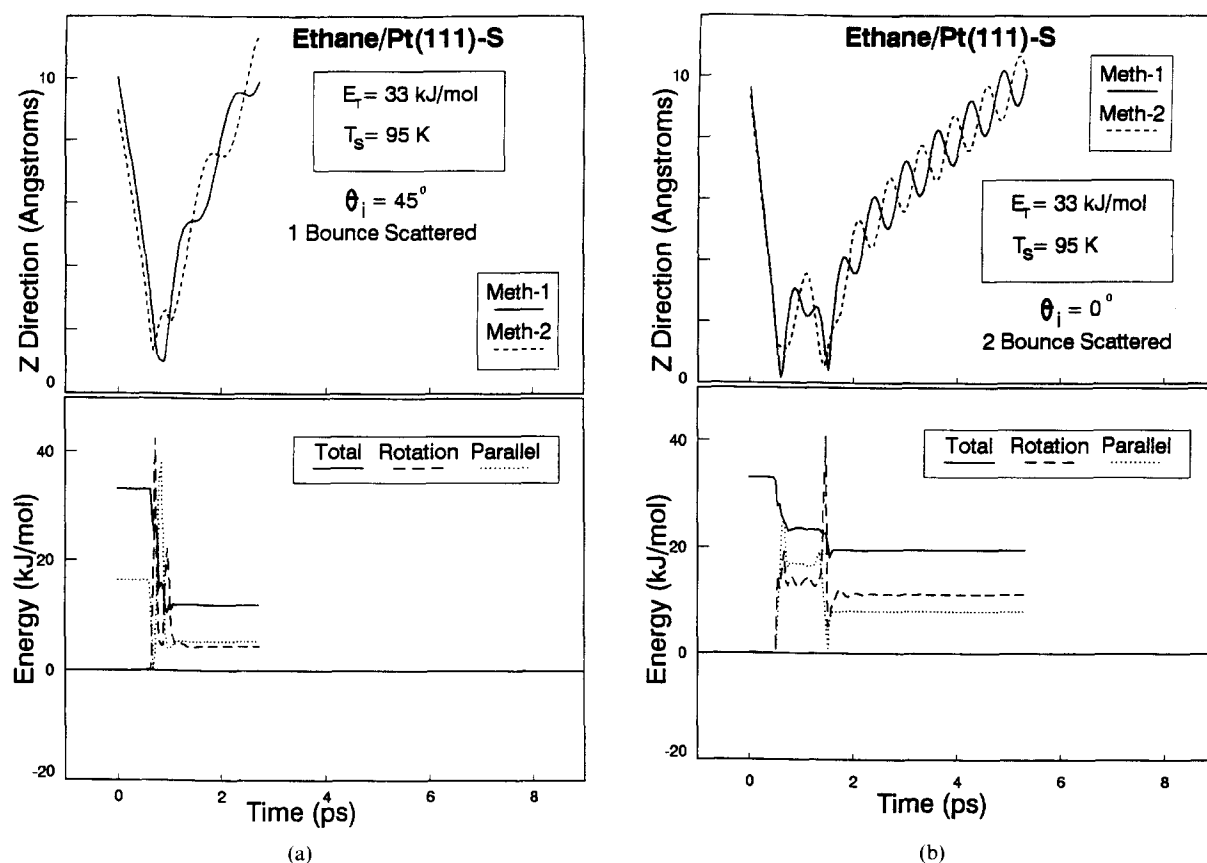


Fig. 14. Single trajectories each incident at Pt(111)-S with  $33 \text{ kJ mol}^{-1}$  of initial translational energy (a) at  $45^\circ$ , and (b) and (c) at  $0^\circ$  from the surface normal. The upper panels show the height above the surface of both methyl groups as a function of time for three single trajectories and the lower panels illustrate the time evolutions of total, rotational and parallel translational energies. The surface temperature is 95 K.

experience a second surface collision. It is by these mechanism(s), particularly conversion of normal to parallel momentum, by which the initial trapping probability at normal incidence of ethane on Pt(111)-S is enhanced relative to that for clean Pt(111). Corrugation plays a large role on the outcome of the subsequent bounce, but with the opposite effect. Upon the second surface collision, ethane loses a sum of almost  $15 \text{ kJ mol}^{-1}$  in parallel and rotational energy, some of which is converted into normal translational energy sufficient to scatter the molecule from the surface. This trajectory indicates the necessity to slowly dissipate energy in each of the energy storage mechanisms in order to trap.

Fig. 14c shows how a trajectory of ethane on

Pt(111)-S that leads to trapping gradually dissipates energy to the surface over a series of collisions. After the first bounce, the energy profile of this trajectory is similar to that of the second trajectory. The difference in fates comes about because this trajectory is better able to slowly dissipate the excited rotational and parallel energy on the second and subsequent bounces. The series of large spikes in the rotational energy (Fig. 14c) occurs from torques on the molecule as it meanders above the surface (Fig. 15). Interestingly, and consistent with the finding of steering, the path of the molecule unquestionably avoids adsorbed sulfur atoms as it wanders around bare platinum regions in a quasi-circular direction before ultimately becoming trapped.

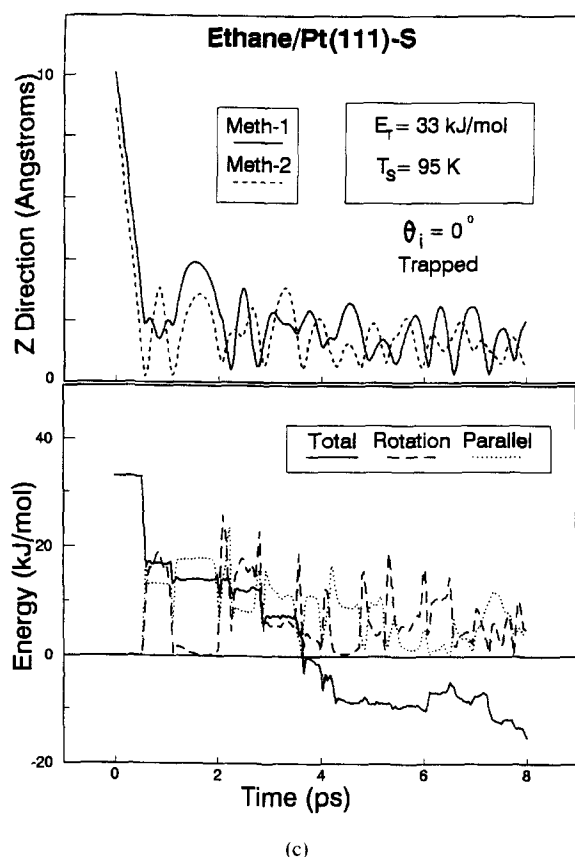


Fig. 14. (continued)

## 7. Summary and conclusions

We have employed supersonic molecular beam experiments and three-dimensional stochastic trajectory simulations to examine the effect of rigidly bound adsorbates on the molecular trapping of ethane. The important conclusions are:

- (1) The direct-inelastic channels of angular distributions for ethane scattering from sulfur- and ethyldiyne-covered Pt(111) are very broad, displaying a high degree of back-scattering. Using the measured initial trapping probabilities for ethane on clean [19] and sulfur-covered [18] Pt(111), excellent agreement was found for the direct-inelastic components of ethane scattering from these surfaces at low and high temperatures, indicating the results from both studies are consistent. Simulations of ethane interacting with Pt(111)-S employing the

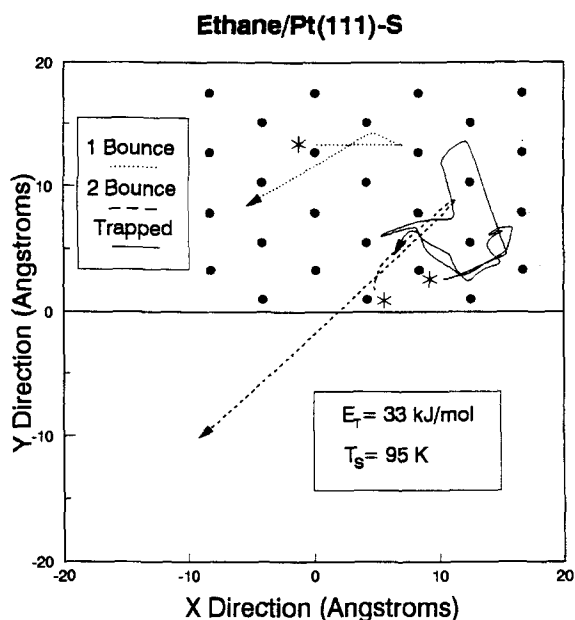


Fig. 15. The path of the center of mass positions for the three single trajectories presented in Figs. 14a–c. The solid circles represent the equilibrium positions of sulfur atoms. The asterisks and arrows indicate the initial and final positions, respectively, above the Pt(111)-S surface for each single trajectory.

Morse potential developed from ethane trapping on and scattering from Pt(111) quantitatively predicts the extremely broad angular distributions of ethane from Pt(111)-S and the total energy scaling for the initial trapping probabilities of this system over the entire range of conditions studied. The simulations also accurately predict the observed differences between ethane on clean Pt(111) and Pt(111)-S.

- (2) Calculations of energy transfer for ethane after the first bounce on Pt(111)-S clearly indicate rapid conversion of parallel and perpendicular momentum for all angles of incidence. At normal incidence, the initial trapping probability for ethane on Pt(111)-S is enhanced relative to clean Pt(111) by the excitation of parallel translational energy, while at glancing angles of incidence ( $\geq 45^\circ$ ), trapping is depressed on the sulfur-covered surface because initial parallel momentum is converted into perpendicular momentum upon the first bounce.

- (3) Multiple bounce scattering of ethane from sulfur-covered Pt(111) was found to be more significant than that from clean Pt(111)–S; the initial trapping probability of ethane on Pt(111)–S is determined to within 20% by the outcome of the first surface collision compared to 10% for clean Pt(111). The primary mechanism for multiple bounce scattering of ethane from Pt(111)–S was found to be conversion of parallel translational momentum into normal momentum, in contrast to Pt(111), which exhibited multiple bounce scattering via reconversion of cartwheel rotational energy to translational energy normal to the surface.
- (4) Analysis of surface impact sites illustrates that ethane incident at all angles is steered away from the adsorbed sulfur atoms into the “bare” platinum regions by the corrugation of the Pt(111)–S surface. This effect produces a scrambling of incident translational motion of ethane and quickly reduces the memory of the initial conditions. The broad angular distributions of ethane scattering from Pt(111)–S and the angle independent initial trapping probabilities for ethane on Pt(111)–S result from this phenomenon.

### Acknowledgements

We gratefully acknowledge Dr John Tully of AT&T Bell Laboratories for discussions in the initial stages of this work and for providing the computer codes that were modified to perform these calculations. We would also like to thank Michael Spaid and Dr George M. Homsy for graciously extending their computer for some of these calculations. Finally, we gratefully acknowledge the Department of Energy, Chemical Sciences Division, Office of Basic Energy Sciences (grant DE-FG03-86ER13468) for financial support of this work.

### References

- [1] J.E. Adams, J.D. Doll, *J. Chem. Phys.* 80 (1984) 1681.
- [2] D. Zhao, J.E. Adams, *Langmuir* 1 (1985) 557.
- [3] D. Zhao, J.E. Adams, *Surf. Sci.* 171 (1986) 208.
- [4] M.P. D'Evelyn, H.-P. Steinrück, R.J. Madix, *Surf. Sci.* 180 (1987) 47.
- [5] C.T. Rettner, E.K. Schweizer, C.B. Mullins, *J. Chem. Phys.* 90 (1989) 3800.
- [6] H.C. Kang, C.B. Mullins, W.H. Weinberg, *J. Chem. Phys.* 92 (1990) 1397.
- [7] H.C. Kang, C.B. Mullins, W.H. Weinberg, *J. Vac. Sci. Technol. A* 8 (1990) 2538.
- [8] C.R. Arumainayagam, M.C. McMaster, R.J. Madix, *Surf. Sci. Lett.* 237 (1990) L424.
- [9] C.R. Arumainayagam, J.A. Stinnett, M.C. McMaster, R.J. Madix, *J. Chem. Phys.* 95 (1991) 5437.
- [10] M. Head-Gordon, J.C. Tully, H. Schlichting, D. Menzel, *J. Chem. Phys.* 95 (1991) 9266.
- [11] M. Head-Gordon, J.C. Tully, *Surf. Sci.* 268 (1992) 113.
- [12] M.C. McMaster, C.R. Arumainayagam, R.J. Madix, *Chem. Phys.* 177 (1993) 461.
- [13] M.C. McMaster, S.L.M. Schroeder, R.J. Madix, *Surf. Sci.* 297 (1993) 253.
- [14] M.C. McMaster, R.J. Madix, *Surf. Sci. Lett.* 293 (1993) L847.
- [15] A.P.J. Jansen, *J. Chem. Phys.* 97 (1992) 5205.
- [16] F. de Jong, A.P.J. Jansen, *Surf. Sci.* 312 (1994) 1.
- [17] S.A. Soulen, J.A. Stinnett, R.J. Madix, *Surf. Sci.* 303 (1994) 312.
- [18] J.A. Stinnett, M.C. McMaster, R.J. Madix, *Surf. Sci.* 364 (1996) 325.
- [19] C.R. Arumainayagam, G.R. Schoofs, M.C. McMaster, R.J. Madix, *J. Phys. Chem.* 95 (1991) 1041.
- [20] C.T. Rettner, D.S. Bethune, D.J. Auerbach, *J. Chem. Phys.* 91 (1989) 1942.
- [21] J.A. Stinnett, R.J. Madix, J.C. Tully, *J. Chem. Phys.* 104 (1996) 3134.
- [22] J.A. Stinnett, M.C. McMaster, S.L.M. Schroeder, R.J. Madix, J.C. Tully, *Surf. Sci.* 365 (1996) 683.
- [23] J.A. Stinnett, R.J. Madix, J.C. Tully, *J. Chem. Phys.* 105 (1996) 1609.
- [24] C.R. Arumainayagam, M.C. McMaster, G.R. Schoofs, R.J. Madix, *Surf. Sci.* 222 (1989) 213.
- [25] A.M. Lahee, J.P. Toennies, Ch. Wöll, *Surf. Sci.* 177 (1986) 371.
- [26] M.P. D'Evelyn, A.V. Hamza, G.E. Gdowski, R.J. Madix, *Surf. Sci.* 167 (1986) 451.
- [27] W. Heegeman, K.H. Meister, E. Bechtold, K. Hayek, *Surf. Sci.* 49 (1975) 161.
- [28] N.M. Abbas, Ph.D. Thesis, Stanford University, CA, 1981.
- [29] K. Hayek, H. Glassl, A. Gutmann, H. Leonhard, M. Prutton, S.P. Tear, M.R. Welton-Cook, *Surf. Sci.* 152/153 (1985) 419.
- [30] R.J. Koestner, M. Salmeron, E.B. Kollin, J.L. Gland, *Chem. Phys. Lett.* 125 (1986) 134.
- [31] R.J. Koestner, M. Salmeron, E.B. Kollin, J.L. Gland, *Surf. Sci.* 172 (1986) 668.
- [32] K. Hayek, H. Glassl, A. Gutmann, H. Leonhard, M. Prutton, S.P. Tear, M.R. Welton-Cook, *Surf. Sci.* 175 (1986) 535.

- [33] M. Kiskinova, A. Szabo, J.T. Yates, Jr., *J. Chem. Phys.* 89 (1988) 7599.
- [34] P.C. Stair, G.A. Somorjai, *J. Chem. Phys.* 66 (1977) 2036.
- [35] A.M. Baro, H. Ibach, *J. Chem. Phys.* 74 (1981) 4194.
- [36] M. Salmeron, G.A. Somorjai, *J. Phys. Chem.* 86 (1982) 341.
- [37] H. Steininger, H. Ibach, S. Lehwald, *Surf. Sci.* 117 (1982) 685.
- [38] N. Freyer, G. Pirug, H.P. Bonzel, *Surf. Sci.* 125 (1983) 327.
- [39] N. Freyer, G. Pirug, H.P. Bonzel, *Surf. Sci.* 126 (1983) 487.
- [40] J.R. Creighton, J.M. White, *Surf. Sci.* 129 (1983) 327.
- [41] J.R. Creighton, K.M. Ogle, J.M. White, *Surf. Sci. Lett.* 138 (1984) L137.
- [42] F. Zaera, G.A. Somorjai, *J. Am. Chem. Soc.* 106 (1984) 2288.
- [43] J.A. Horsley, J. Stöhr, R.J. Koestner, *J. Chem. Phys.* 83 (1985) 3146.
- [44] D. Godbey, F. Zaera, R. Yeates, G.A. Somorjai, *Surf. Sci.* 167 (1986) 150.
- [45] K.M. Ogle, J.M. White, *Surf. Sci.* 165 (1986) 234.
- [46] M. Abon, J. Billy, J.C. Bertolini, *Surf. Sci.* 171 (1986) L387.
- [47] R. Yu, T. Gustafsson, *Surf. Sci. Lett.* 182 (1987) L234.
- [48] F. Zaera, *J. Am. Chem. Soc.* 111 (1989) 4240.
- [49] F. Zaera, *J. Chem. Phys.* 94 (1990) 5090.
- [50] I.V. Mitchell, W.N. Lennard, K. Griffiths, G.R. Massoumi, J.W. Huppertz, *Surf. Sci. Lett.* 256 (1991) L598.
- [51] K. Griffiths, W.N. Lennard, I.V. Mitchell, P.R. Norton, G. Pirug, H.P. Bonzel, *Surf. Sci. Lett.* 284 (1993) L389.
- [52] U. Starke, A. Barbieri, N. Materer, M.A. Van Hove, G.A. Somorjai, *Surf. Sci.* 286 (1993) 1.
- [53] G.E. Gdowski, Ph.D. Thesis, Stanford University, CA, 1985.
- [54] M.P. D'Evelyn, A.V. Hamza, G.E. Gdowski, R.J. Madix, *Surf. Sci.* 167 (1986) 451.
- [55] J.E. Hurst, L. Wharton, K.C. Janda, D.J. Auerbach, *J. Chem. Phys.* 78 (1983) 1559.
- [56] H. Asada, *Jap. J. Appl. Phys.* 20 (1981) 527.
- [57] J.C. Tully, *Acc. Chem. Res.* 14 (1981) 188.
- [58] J.C. Tully, Simulation of gas-surface dynamics, in: D. Langreth and H. Suhl (Eds.), *Many Body Phenomena at Surfaces*, Academic, New York, 1984, p. 377.
- [59] M. Head-Gordon, J.C. Tully, C.T. Rettner, B. Mullins, D.J. Auerbach, *J. Chem. Phys.* 94 (1991) 1516.
- [60] C.R. Arumainayagam, R.J. Madix, M.C. McMaster, V.M. Suzawa, J.C. Tully, *Surf. Sci.* 226 (1990) 180.
- [61] S.A. Adelman, J.D. Doll, *J. Chem. Phys.* 64 (1976) 2375.
- [62] J.R. Harris, N. Benczer-Koller, G.M. Rothberg, *Phys. Rev. A* 137 (1965) 1101.
- [63] C. Kittel, *Introduction to Solid State Physics*, 6th ed., Wiley, New York, 1986, p. 110.
- [64] G. Herzberg, *Infrared and Raman Spectra*, Van Nostrand, New York, 1945.
- [65] J.C. Tully, G.H. Gilmer, M. Shugard, *J. Chem. Phys.* 71 (1979) 1630.
- [66] S. Anderson, J. Harris, *Phys. Rev. B* 27 (1983) 9.
- [67] J.P. Cowin, C.-F. Yu, S.J. Sibener, J.E. Hurst, *J. Chem. Phys.* 75 (1981) 1033.
- [68] C.-F. Yu, K.B. Whaley, C.S. Hogg, S.J. Sibener, *Phys. Rev. Lett* 51 (1983) 2210.
- [69] J.P. Cowin, C.-F. Yu, S.J. Sibener, L. Wharton, *J. Chem. Phys.* 79 (1983) 3537.
- [70] C.-Y. Lee, R.F. Grote, A.E. DePristo, *Surf. Sci.* 145 (1984) 466.
- [71] A.E. DePristo, *Surf. Sci.* 137 (1984) 130.
- [72] C.-F. Yu, K.B. Whaley, C.S. Hogg, S.J. Sibener, *J. Chem. Phys.* 83 (1985) 4217.
- [73] K.B. Whaley, C.-F. Yu, C.S. Hogg, J.C. Light, S.J. Sibener, *J. Chem. Phys.* 83 (1985) 4235.
- [74] C.-Y. Lee, A.E. DePristo, *J. Chem. Phys.* 87 (1987) 1401.
- [75] C.T. Rettner, L.A. DeLouise, J. P. Cowin, D.J. Auerbach, *Chem. Phys. Lett.* 118 (1985) 355.
- [76] C.T. Rettner, L.A. DeLouise, J.P. Cowin, D.J. Auerbach, *Fara. Discuss. Chem. Soc.* 80 (1985) 127.
- [77] J.C. Polanyi, R.J. Wolf, *Ber. Bunsenges Phys. Chem.* 86 (1982) 356.
- [78] J.C. Polanyi, R.J. Wolf, *J. Chem. Phys.* 82 (1985) 1555.
- [79] R.J. Wolf, R.C. Davis, *J. Phys. Chem.* 89 (1985) 2757.
- [80] C.W. Muhlhausen, L.R. Williams, J.C. Tully, *J. Chem. Phys.* 83 (1985) 2594.
- [81] J. Harris, A.C. Luntz, *J. Chem. Phys.* 91 (1989) 6421.
- [82] D.C. Jacobs, K.W. Kolasinski, R.J. Madix, R.N. Zare, *J. Vac. Sci. Technol. A* 7 (1989) 1871.
- [83] D.C. Jacobs, R.N. Zare, *J. Chem. Phys.* 91 (1989) 3196.
- [84] M.A. Hines, R.N. Zare, *J. Chem. Phys.* 98 (1993) 9134.
- [85] J. Kimman, C.T. Rettner, D.J. Auerbach, J.A. Barker, J.C. Tully, *Phys. Rev. Lett.* 57 (1986) 2053.
- [86] C.T. Rettner, J. Kimman, F. Fabre, D.J. Auerbach, J.A. Barker, J.C. Tully, *J. Vac. Sci. Technol. A* 5 (1987) 508.
- [87] R.J. Smith, A. Kara, S. Holloway, *Surf. Sci.* 269270 (1992) 158.
- [88] D.P. Masson, T.F. Hanisco, W.L. Nichols, C. Yan, A.C. Kummel, *J. Chem. Phys.* 101 (1994) 3341.
- [89] R.M. Logan, R.E. Stickney, *J. Chem. Phys.* 44 (1966) 195.
- [90] R.M. Logan, J.C. Keck, *J. Chem. Phys.* 49 (1968) 860.
- [91] W.L. Nichols, J.H. Weare, *J. Chem. Phys.* 62 (1975) 3754.
- [92] M. Persson, J. Harris, *Surf. Sci.* 187 (1987) 67.
- [93] J.C. Tully, *J. Chem. Phys.* 92 (1990) 680.